OXFORD

*Human Molecular Genetics*, 2023, Vol. 32, 12, 2055–2067
https://doi.org/10.1093/hmg/ddad041
Advance access publication date 14 March 2023
**Original Article**

# Genetic modifiers modulate phenotypic expression of tafazzin deficiency in a mouse model of Barth syndrome

Suya Wang[1], Erika Yazawa[2], Erin M. Keating[1], Neil Mazumdar[1], Alexander Hauschild[1], Qing Ma[1], Haiyan Wu[3], Yang Xu[4], Xu Shi[5], Douglas Strathdee[6], Robert E. Gerszten[5], Michael Schlame[4] and William T. Pu[1,6,7,*]

[1]Department of Cardiology, Boston Children's Hospital, Boston, MA 02215NYU 10016, USA
[2]Division of Newborn Medicine, Boston Children's Hospital, Boston, MA 02215NYU 10016, USA
[3]Department of Pharmacology, Sichuan University West China School of Basic Sciences and Forensic Medicine, Chengdu, Sichuan, China
[4]Department of Anesthesiology, New York University School of Medicine, New York, NY, USA
[5]Division of Cardiovascular Medicine, Beth Israel Deaconess Medical Center, Boston, MA 02115, USA
[6]Transgenic Technology Laboratory, Cancer Research UK Beatson Institute, Glasgow, UK
[7]Harvard Stem Cell Institute, Harvard University, 02138 Beatson, Cambridge, MA G61 1BD, USA

*To whom correspondence should be addressed at: 300 Longwood Ave, Boston, MA 02115, USA. Tel: +1 6179192091; Email: william.pu@cardio.chboston.org

## Abstract

Barth syndrome is an X-linked disorder caused by loss-of-function mutations in Tafazzin (*TAZ*), an acyltransferase that catalyzes remodeling of cardiolipin, a signature phospholipid of the inner mitochondrial membrane. Patients develop cardiac and skeletal muscle weakness, growth delay and neutropenia, although phenotypic expression varies considerably between patients. *Taz* knockout mice recapitulate many of the hallmark features of the disease. We used mouse genetics to test the hypothesis that genetic modifiers alter the phenotypic manifestations of *Taz* inactivation. We crossed $Taz^{KO/X}$ females in the C57BL6/J inbred strain to males from eight inbred strains and evaluated the phenotypes of first-generation (F1) $Taz^{KO/Y}$ progeny, compared to $Taz^{WT/Y}$ littermates. We observed that genetic background strongly impacted phenotypic expression. C57BL6/J and CAST/EiJ[F1] $Taz^{KO/Y}$ mice developed severe cardiomyopathy, whereas A/J[F1] $Taz^{KO/Y}$ mice had normal heart function. C57BL6/J and WSB/EiJ[F1] $Taz^{KO/Y}$ mice had severely reduced treadmill endurance, whereas endurance was normal in A/J[F1] and CAST/EiJ[F1] $Taz^{KO/Y}$ mice. In all genetic backgrounds, cardiolipin showed similar abnormalities in knockout mice, and transcriptomic and metabolomic investigations identified signatures of mitochondrial uncoupling and activation of the integrated stress response. $Taz^{KO/Y}$ cardiac mitochondria were small, clustered and had reduced cristae density in knockouts in severely affected genetic backgrounds but were relatively preserved in the permissive A/J[F1] strain. Gene expression and mitophagy measurements were consistent with reduced mitophagy in knockout mice in genetic backgrounds intolerant of *Taz* mutation. Our data demonstrate that genetic modifiers powerfully modulate phenotypic expression of *Taz* loss-of-function and act downstream of cardiolipin, possibly by altering mitochondrial quality control.

## Introduction

Deleterious variants in Tafazzin (*TAZ*), an acyltransferase that catalyzes the remodeling of cardiolipin (CL) (1), cause Barth syndrome, an X-linked disorder with hallmark features of cardiomyopathy (CMP), skeletal myopathy and neutropenia (OMIM: #302060) (2–5). CL is a signature lipid of the inner mitochondrial membrane (IMM) and has been implicated in IMM folding into cristae (6) and the packing and function of IMM proteins (7) including the electron transport chain and the F1F0-ATPase. The mechanistic links between impaired *TAZ* function and its characteristic manifestations remain poorly understood, but include impaired electron transport chain and F1F0-ATPase activity, excessive generation of reactive oxygen species and $Ca^{2+}$-calmodulin dependent kinase activation, and aberrant cytosolic and mitochondrial $Ca^{2+}$ handling (8–11).

While Barth syndrome is an ultra-rare disorder, abnormalities of CL composition have been reported in common acquired diseases such as diabetes and heart failure (12). In addition to its biophysical roles in mitochondrial cristae structure and stabilizing respiratory supercomplexes (6,13,14), CL has been implicated in fundamental processes including mitochondrial fusion, mitophagy and apoptosis, through its interactions with OPA1, LC3 and cytochrome C (15–18). Thus, TAZ deficiency provides a window in central biological processes and the pathophysiology of common, highly prevalent diseases.

Barth syndrome patients exhibit wide phenotypic variation. For example, many patients have mild cardiac involvement, but ~15% have involvement severe enough to require heart transplantation (4). Skeletal myopathy likewise has variable expressivity, with fatigue symptoms severe enough in some individuals to limit employment opportunities and require mobility aids (4). No obvious relation between the type or site of TAZ variants and phenotypic expression has been identified. Phenotypic variations within family members with the same pathogenic variant further argue against the *TAZ* genotype being the primary driver of phenotypic variation.

Variation in other genes that modify the expression of *TAZ* mutation may contribute to the phenotypic variation observed in Barth syndrome patients. Discovery of these modifiers would provide insights into TAZ and CL homeostatic mechanisms, and provide new avenues for the development of therapeutics for Barth syndrome. Here, we used mouse genetics to test the

**Received:** January 31, 2023. **Revised:** February 27, 2023. **Accepted:** March 9, 2023

hypothesis that genetic modifiers alter the phenotypic manifestations of Barth syndrome. We demonstrate that genetic modifiers powerfully govern phenotypes caused by *Taz* knockout (KO).

## Results

We previously characterized *Taz* KO mice on a C57BL6/J background (C57/J) and showed that $Taz^{KO/Y}$ males suffer from perinatal lethality (19). Survivors developed progressive, severe dilated CMP and severe limitation to treadmill exercise. To investigate the effect of strain background, we crossed $Taz^{KO/X}$ female carriers to wild-type (WT) males from eight different inbred strains (Fig. 1A): C57/J, CAST/EiJ (CAST), 129S1/SvlmJ (129S1), A/J, NOD/ShiLtJ (NOD), NZO/HLLtJ (NZO), PWK/PhJ (PWK) and WSB/EiJ (WSB). These inbred strains were selected because they are the founder strains for Diversity Outbred mice, an outbred population designed for efficient genetic modifier mapping (20). We studied first generation (F1) progeny from this cross to assess neonatal survival, somatic growth, heart function, skeletal muscle function, CL composition and mitochondrial morphology and dynamics. Since *Taz* is X-linked, we analyzed male mice with genotypes $Taz^{KO/Y}$ (KO) and $Taz^{WT/Y}$ (WT).

### Survival and somatic growth

Survival to birth was assessed by genotyping F1 progeny on the day of birth. $Taz^{KO/Y}$ mice were present at sub-Mendelian frequency in the C57/J background (Fig. 1B). In all of the F1 backgrounds, survival did not differ significantly from the expected Mendelian frequency. However, birth weight was significantly reduced compared to littermate controls in all $Taz^{KO/Y}$ pups, with the most striking reduction in birth weight occurring in KO-C57/J[F1] (~30% reduction) and the least reduction occurring in KO-A/J[F1] (~7%) (Fig. 1C). We examined subsequent survival to weaning (Fig. 1D). Survival was significantly reduced only in KO-C57/J[F1], although there were two deaths between 15 and 30 days in KO-129S1[F1] and one in KO-NZO[F1], a period during which no WT littermates died.

Barth patients show delayed somatic growth in childhood but often experience delayed puberty and as a result achieve a normal or even tall stature (3). In contrast, $Taz^{KO/Y}$ mice were smaller than their littermate controls from birth through at least 7 months of age (Fig. 1E). This reduced weight was observed in all strains, including A/J. To assess the effect of *Taz* deficiency on body mass composition, we performed dual x-ray absorptiometry (DEXA) scanning at 2 months of age in A/J[F1], CAST[F1] and NZO[F1]. We observed no difference between KO and WT in fractional lean or fat weight (Supplementary Material, Fig. S1A). NZO is a frequently used model of obesity, and the degree of obesity increases with age (21). Therefore, we also analyzed KO-NZO[F1] and littermate WT-NZO[F1] mice at 5 months of age, when obesity is readily apparent. At this age, we observed that KO-NZO[F1] had the same percentage of fat at 2 and 5 months of age, whereas WT-NZO[F1] increased their percentage of fat by over 70% during this time (Supplementary Material, Fig. S1A and B), so that at 5 months, KO-NZO[F1] mice were significantly more lean than their WT littermates. These data suggest that in at least some genetic backgrounds *Taz* deficiency prevents excess accumulation of adipose tissue.

These data indicate that *Taz* KO mice have decreased embryonic and postnatal survival in selected strain backgrounds, most notably C57/J. Growth impairment caused by *Taz* deficiency is observed in mouse models, with relatively less effect of strain background. However, murine *Taz* KO does not recapitulate the 'catch up growth' observed in human Barth patients due to delayed puberty.

### Cardiac function

One of the hallmark features of Barth syndrome is CMP (5). We previously showed that $Taz^{KO/Y}$ C57/J mice develop ventricular dysfunction that is detectable by echocardiography at approximately 10 weeks of age and progresses with age (19). To assess the effect of genetic background on heart function, we performed echocardiograms on $Taz^{KO/Y}$ and $Taz^{WT/Y}$ littermates in C57/J and F1 genetic backgrounds monthly from 1 to 7 months of age (Fig. 2B). C57/J mice developed severe left ventricular (LV) dysfunction [fractional shortening (FS) KO 27% versus WT 49%]. CAST[F1] KO mice were even more severely affected (FS 10% versus WT 50%). Remarkably, KOs in two strains, 129S1[F1] and A/J[F1], did not exhibit myocardial dysfunction. KOs in the remaining strains (NOD[F1], NZO[F1], PWK[F1] and WSB[F1]) demonstrated more mild or slowly progressive cardiac dysfunction. Severe myocardial dysfunction was reflected by LV dilatation in KO-C57/J and KO-CAST[F1] (Fig. 2B). KO-PWK[F1] mice developed mild LV dilatation, while *Taz* deficiency in the remaining strains did not cause LV dilatation.

Following euthanasia at 7 months of age, we analyzed heart size and fibrosis. Heart weight normalized to body weight (HW/BW) was similar between KO and WT littermates, except for severe cardiomegaly in KO-CAST[F1], consistent with this genetic background having the most severe cardiac dysfunction (Fig. 2C). HW/BW was also slightly mildly elevated in KO-C57/J, although this did not reach statistical significance at this sample size.

These data demonstrate that genetic factors powerfully modify the effect of *Taz* deficiency on cardiac function, with C57/J and CAST[F1] being most severely affected, and 129S1[F1] and A/J[F1] being remarkably unaffected.

### Exercise capacity

A major challenge for Barth syndrome patients is fatigue with relatively little exertion (2,4), which is likely due to reduced ability to augment oxygen consumption during exercise (22) and may reflect a combination of reduced cardiac reserve with skeletal muscle impairment. We used treadmill running to measure exercise capacity of KO and WT littermates on different strain backgrounds at 7 months of age. We used a sub-maximal treadmill protocol in which most mice in most strain backgrounds were able to complete the test. There was a remarkable range of treadmill endurance, with KO-C57/J having the most severely reduced endurance compared to littermates (Fig. 3A). $Taz^{KO/Y}$ in NZO[F1] was similarly impaired, but littermate controls also had reduced endurance, potentially due to obesity. Interestingly, treadmill endurance was dissociated from cardiac function, since KO-CAST[F1] mice had the worst heart function but no reduction of treadmill endurance in our testing protocol, while KO-WSB[F1] mice had substantial exercise limitation with only mild cardiac dysfunction.

To further assess the impact of *Taz* deficiency on skeletal muscle in different strain backgrounds, we performed histological analysis of the quadriceps muscle from 7-month-old mice. We measured myofiber cross-sectional area by using wheat germ agglutinin (WGA) to outline myofiber membranes. Myofiber cross-sectional area was reduced in KO mice in all of the strain backgrounds except NZO[F1]. However, the degree of impairment to treadmill exercise did not correlate with the severity of reduced myofiber size, indicating that myofiber size alone is not a primary determinant of treadmill endurance.

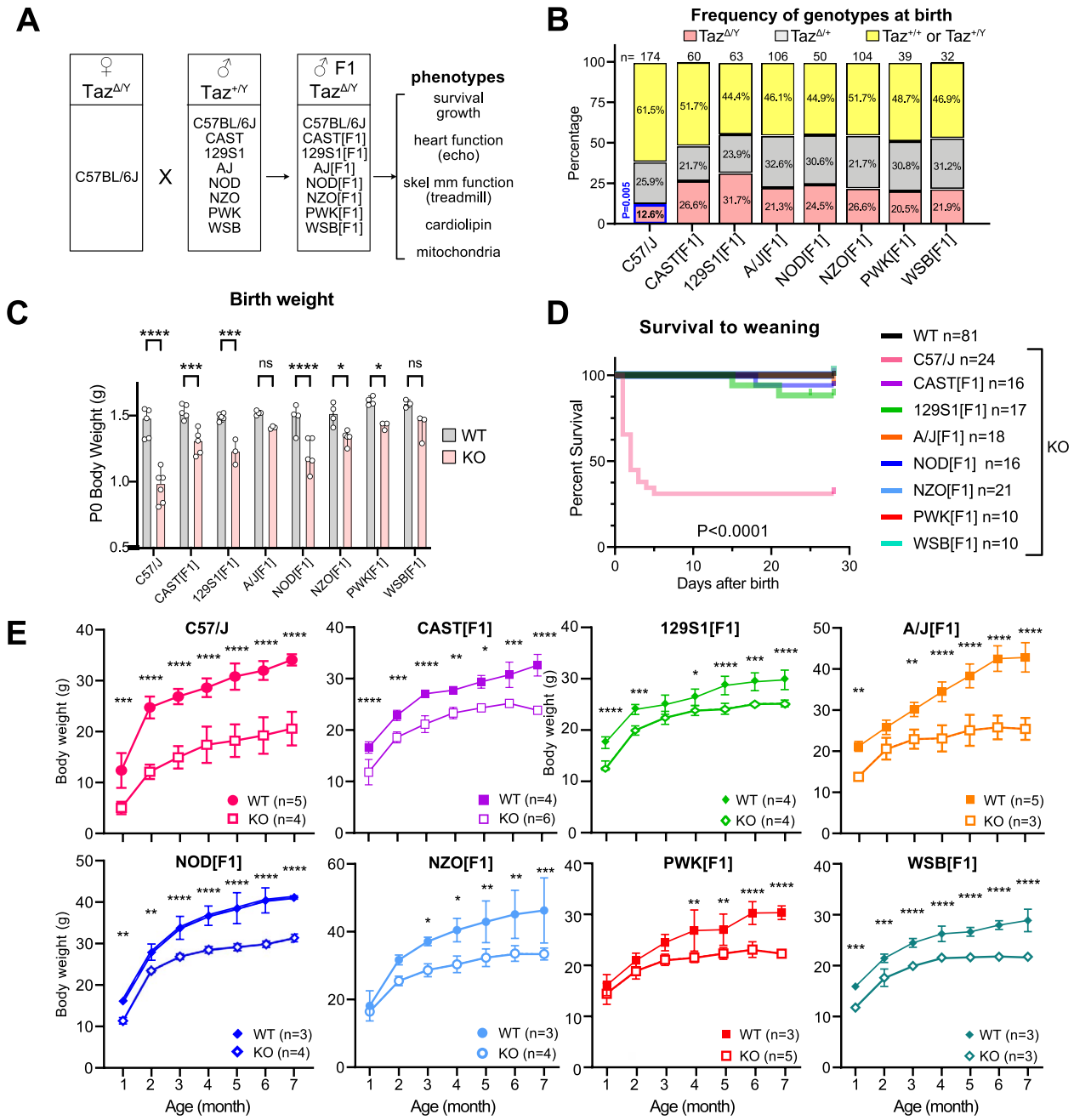


**Figure 1.** Effect of *Taz* KO in different genetic backgrounds on survival and growth. (**A**) Experimental strategy. Carrier females in a C57/J background were crossed to males from eight indicated inbred strains. F1 mutant males were evaluated for multiple phenotypes compared to F1 WT male littermates. (**B**) Genotype frequency at birth. Chi-squared test comparing $Taz^{KO/Y}$ to $Taz^{KO/+}$ within each strain. (**C**) Relative birthweights between male KO and littermate controls. Values were normalized within each litter so that littermate controls had an average value of 1 (dotted line). Two-way analysis of variance (ANOVA) with Šidák's multiple comparison test. (**D**) Survival to weaning. Mantel-Cox test. (**E**) Growth curve of $TAZ^{\Delta/Y}$ and littermate $TAZ^{+/Y}$ mice. Data are shown as mean ± SD. Two-way ANOVA with Šidák's multiple comparison test. *P*-value indicates the effect of genotype at each time point. *, $P < 0.05$; **, $P < 0.01$; ***, $P < 0.001$; ****, $P < 0.0001$.

These results show that genetic factors also strongly influence the effect of *Taz* deficiency on endurance and skeletal muscle phenotypes. The C57/J and WSB[F1] strains were least permissive for *Taz* deficiency, while CAST[F1] and A/J[F1] permitted *Taz* deficiency without observable impairment of endurance in our testing protocol. There was a notable dissociation between cardiac and treadmill endurance phenotypes, suggesting that cardiac limitation is not the major driver of exercise limitation in the treadmill test.

## CL composition and mitochondrial respiratory complexes

TAZ is an acyltransferase that catalyzes remodeling of CL by transferring fatty acids from phospholipids to monolysocardiolipin (MLCL) (1). In *Taz* deficiency, CL levels are low, MLCL levels are high and the MLCL/CL ratio is elevated (1). CL is necessary for normal function of IMM enzymes and for the assembly of respiratory supercomplexes (13,14). To determine if the impact of genetic modifiers in different strain backgrounds occurs

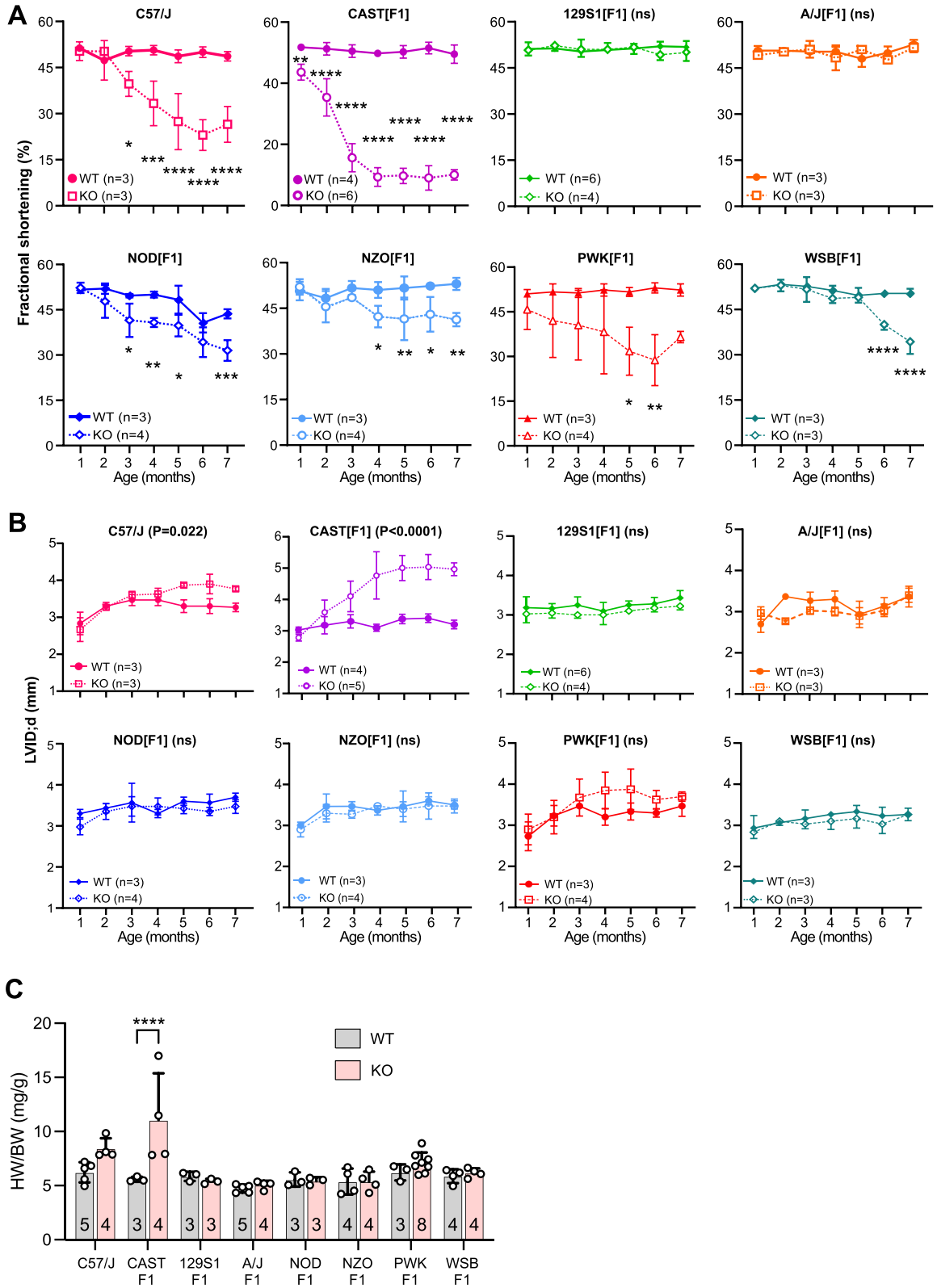


**Figure 2.** Effect of *Taz* KO in different genetic backgrounds on cardiac function. (**A**, **B**) Echocardiography was performed monthly on unsedated mice. Heart function (FS, A) and size (LV internal diameter at end diastole, B) were compared between $Taz^{KO/Y}$ and $Taz^{+/Y}$ littermate controls. Two-way analysis of variance (ANOVA) with Šidák's multiple comparison test. *P*-value indicates the effect of genotype. (**C**) HW/BW ratio at 7 months of age. Two-way ANOVA with Šidák's multiple comparison test. Samples sizes are indicated at the bottom of each bar. *, $P < 0.05$; **, $P < 0.01$; ***, $P < 0.001$; ****, $P < 0.0001$.

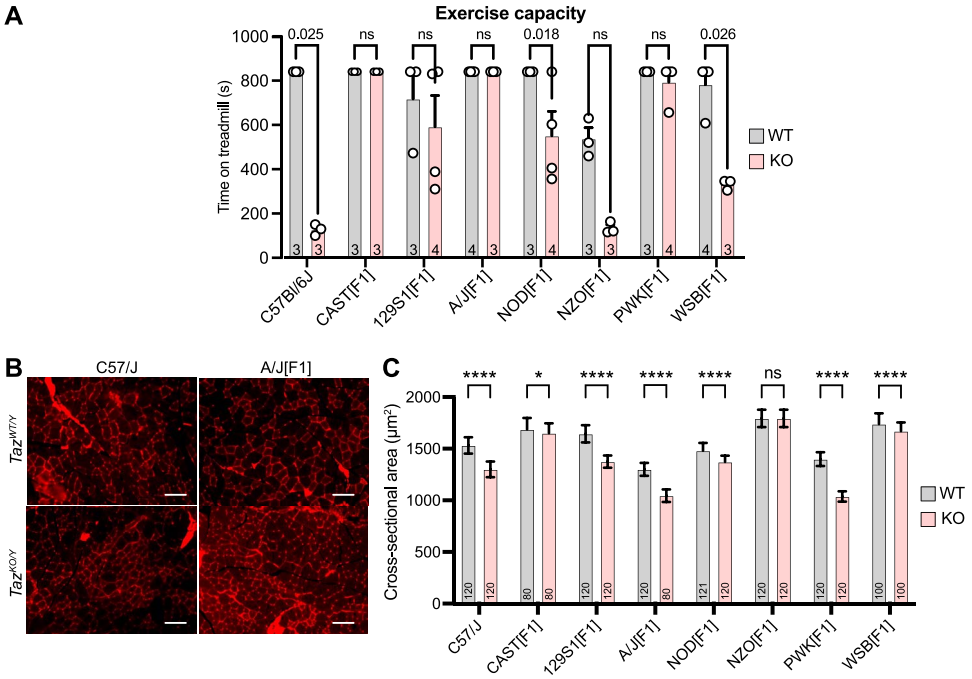


**Figure 3.** Effect of *Taz* KO in different genetic backgrounds on treadmill endurance and skeletal muscle. (**A**) Treadmill endurance. Mice were subjected to exercise challenge on a treadmill (see the Materials and Methods section). Time on treadmill was recorded. The test was stopped at 840 s. Survival to completion of the test was compared between $Taz^{KO/Y}$ and $Taz^{WT/Y}$ littermates using the Mantel-Cox test. (**B**, **C**). Skeletal muscle cross-sectional area. (B) Representative WGA-stained sections of the quadriceps muscle from KO and WT in C57/J (low endurance) and A/J[F1] (normal endurance) strains are shown. Bar, 100 $\mu$m. (C) Quantification of representative images from at least three mice per group. Number at bottom of each bar indicates number of muscle fibers quantified. Two-way analysis of variance with Šidák's multiple comparison test between genotypes within each strain. *, $P < 0.05$; **, $P < 0.01$; ***, $P < 0.001$; ****, $P < 0.0001$.

upstream or downstream of abnormal CL composition, we used Matrix Assisted Laser Desorption/Ionization-Time of Flight Mass Spectrometry to measure CL and MLCL levels and compositions in ventricular tissue from 2-month-old mice (Fig. 4A). Across different genetic backgrounds, we observed similarly reduced CL, increased MLCL and elevated MLCL/CL in $Taz^{KO/Y}$ compared to $Taz^{WT/Y}$ littermates. Specifically, similar abnormalities in CL, MLCL and MLCL/CL were observed in strains with low (A/J) and high (C57/J) phenotypic expression. These data indicate that genetic modifiers modulate phenotypic expression downstream of CL abnormalities.

*Taz* deficiency has previously been shown to reduce levels of components of mitochondrial respiratory complexes. We used an antibody panel against several subunits of respiratory complexes I-V to measure their levels by capillary western in two non-permissive (C57/J and CAST[F1]) and one permissive (A/J[F1]) strains (Fig. 4B). We observed reduced cellular levels of SDHB (Complex II) and ATP5A (Complex V) in all strains, although the degree of reduction was greater in KO-C57/J and KO-CAST[F1] than in KO-A/J[F1]. NDUFB8 (Complex I), UQCRC2 (Complex III) and MT-CO1 (Complex IV) were reduced in KO-C57/J[F1] and KO-CAST[F1], but not KO-A/J[F1]. These data indicate that TAZ and CL abnormalities have strain-dependent effects on respiratory complexes that correlate with the severity of observed phenotypes.

## Transcriptomic and metabolomic analysis of TAZ deficiency in permissive and non-permissive genetic backgrounds

To further investigate the effects of *Taz* deficiency in permissive and non-permissive genetic backgrounds, we performed RNA-seq on 2-month-old $Taz^{KO/Y}$ and $Taz^{WT/Y}$ hearts in non-permissive (C57/J and CAST[F1]) and permissive (A/J[F1]) strain backgrounds (Fig. 5A; Supplementary Material, Table S1). Due to reduced survival of the germline $Taz^{KO/Y}$ mice in the C57/J background, the RNA-seq experiment for this strain used cardiac-selective KO of a conditional (loxP-flanked) *Taz* allele ($Taz^{flox}$) by cardiac-specific *Myh6Cre*. Upon Cre recombination, excision of the floxed region yields the same $Taz^{KO}$ allele used elsewhere in this study. We previously showed that $Taz^{flox/Y}$; *Myh6Cre* mice in the C57/J background have a similar cardiac phenotype to $Taz^{KO/Y}$ mice in the same background (19). Principal component analysis of three to four biological replicates per group showed that replicate samples clustered together (Supplementary Material, Fig. S2A). Principal component 1 separated samples by *Taz* genotype. Principal component 2 separated samples by strain regardless of genotype: CAST[F1] was widely separated from C57/J and A/J, reflecting its greater genetic separation as a wild-derived strain (23).

To facilitate data analysis, we pooled the two non-permissive strains in which *Taz* deficiency caused cardiac dysfunction and labeled this pooled virtual strain as 'CMP'. This led to four potential pairwise comparisons (Fig. 5B). In each comparison, we defined differentially expressed genes (DEGs) as $P_{adj} < 0.05$ and absolute $\log_2$ fold-change >0.58 (50%). Within either A/J[F1] or CMP, we identified over 2500 DEGs between KO and WT, whereas analysis for strain differences within either KO or WT yielded relatively few (~300) DEGs. A scatterplot of expression changes between KO and WT in either A/J[F1] or CMP strains showed that most changes correlated (black points, Fig. 5C; Supplementary Material, Table S1). Other genes were DEGs exclusively in either A/J[F1] or CMP (blue or green, respectively, Fig. 5C); in most cases, these genes showed similar direction of change in expression between KO and WT, but differed in the magnitude of change. A small number of genes were identified as exhibiting interaction between *Taz* genotype and strain background (red, Fig. 5C).

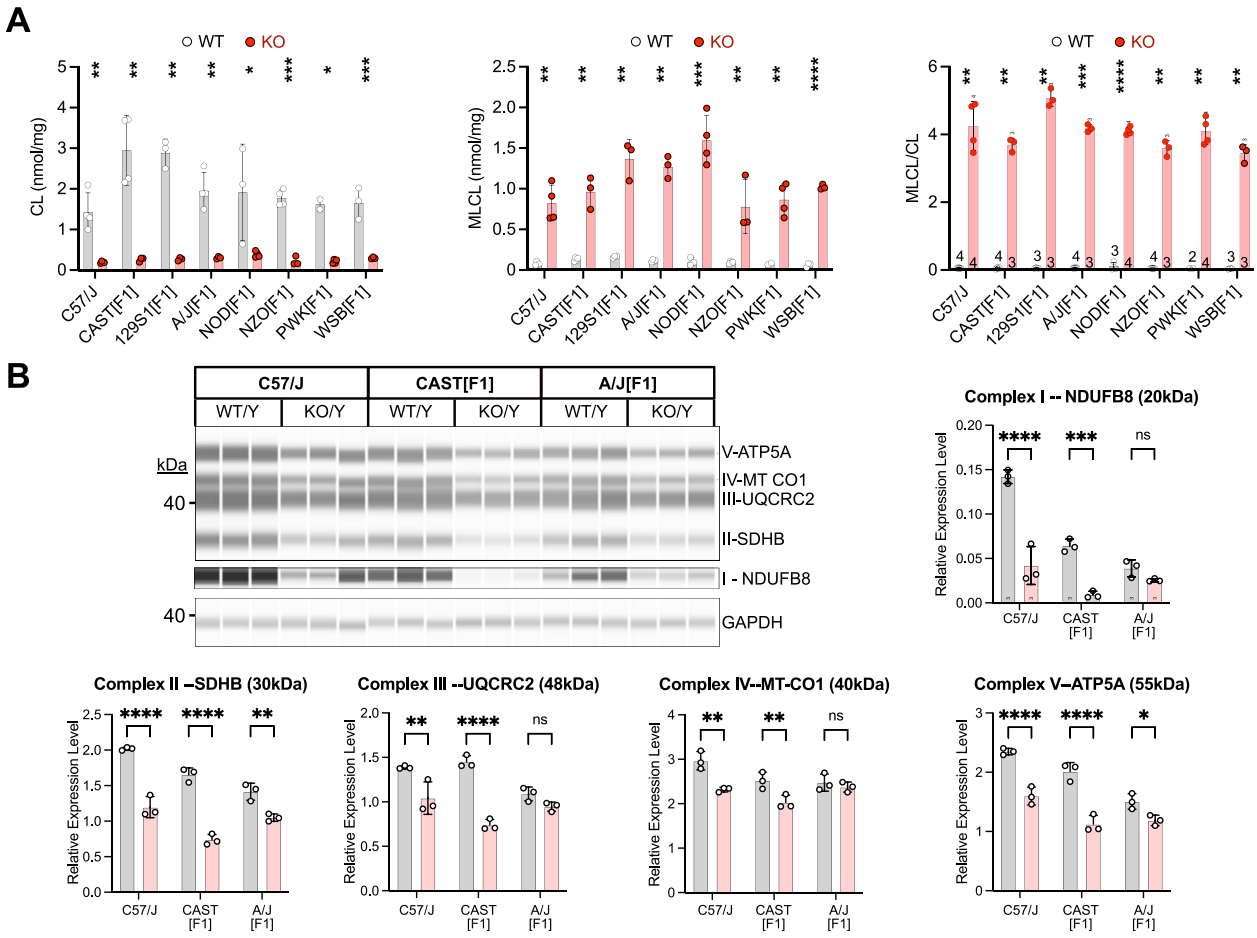


**Figure 4.** Effect of *Taz* KO in different genetic backgrounds on CL composition and expression of mitochondrial respiratory complexes. (**A**) CL composition of $Taz^{\Delta/Y}$ and $Taz^{+/Y}$ 2-month-old mouse hearts. CL and MLCL compositions were determined by mass spectrometry and normalized to total protein. Sample sizes are indicated in the right most plot. Welch's *t*-test with BH multiple testing correction. (**B**) Mitochondrial respiratory complex composition was evaluated by capillary western blotting. Whole heart lysates were probed with an antibody panel to the indicated protein components of complexes I–V and to GAPDH. Relative level of each protein was determined from the capillary western and normalized to GAPDH. Two-way analysis of variance with Šidák's multiple comparison test. ns, $P \geq 0.05$; *, $P < 0.05$; **, $P < 0.01$; ***, $P < 0.001$; ****, $P < 0.0001$.

We examined the biological process terms that were enriched by each pairwise comparison, using Gene Set Enrichment Analysis (Fig. 5D) (24). Contrasts between KO and WT in either the A/J[F1] or CMP strains yielded similar functional terms: upregulated genes were enriched for terms related to ribosome biogenesis and translation, whereas downregulated genes were enriched for terms related to fatty acid oxidation, adrenergic receptor signaling, heart rate and contraction and vascular development. A set of terms related to mRNA processing were uniquely enriched in KO-upregulated genes in A/J[F1]. A complimentary analysis of functional terms over-represented for DEGs between KO versus WT in either CMP or A/J[F1] also identified enrichment of 'Ribosome', 'Aminoacyl-tRNA biosynthesis', 'Translation factors' and 'Cytoplasmic ribosomal proteins', suggesting abnormalities in ribosomes and protein translation (Supplementary Material, Fig. S2B). Other terms enriched for upregulated genes included 'One carbon pool by folate' and 'Glycine, serine, and threonine metabolism'. Among downregulated genes, 'Fatty acid oxidation' was enriched in both strains (Supplementary Material, Fig. S2B). However, some metabolic terms such as 'Fatty acid beta oxidation', 'mitochondrial long chain fatty acid beta oxidation' and Propanoate metabolism" were enriched for downregulated genes in CMP and not A/J[F1].

Contrasts between CMP versus A/J[F1] in either KO or WT genotypes identified biological processes differentially regulated between strains. Genes upregulated in CMP versus A/J[F1] in WT included the same set of mRNA processing terms found in KO-upregulated genes in A/J[F1], as well as ribosome biogenesis terms enriched in KO-upregulated genes in both strains. In contrast, genes upregulated in CMP versus A/J[F1] in KO were enriched for terms related to integrin signaling, proteasomal ubiquitin-independent protein catabolism and hemostasis. Among genes downregulated in CMP versus A/J[F1], 'heart contraction' was enriched in both KO and WT genotypes, while carbohydrate transport and glycosaminoglycan synthesis were enriched in WT and TGF$\beta$ receptor signaling and NADH metabolic process terms were enriched in KO.

To gain further insights from the transcriptome profiling data, we integrated our data with the Ingenuity Knowledge Base, which incorporates manually curated pathways from thousands of gene expression datasets. Using this knowledge base and a strategy to find causative upstream regulators (25), we identified a set of key upstream 'master regulators'. Activation of UCP1 and ATF4 was predicted to be shared between both A/J[F1] and CMP strains (Fig. 5E). These findings were highly significant, as the 'activity score' assigned to UCP1 was the highest among several thousands

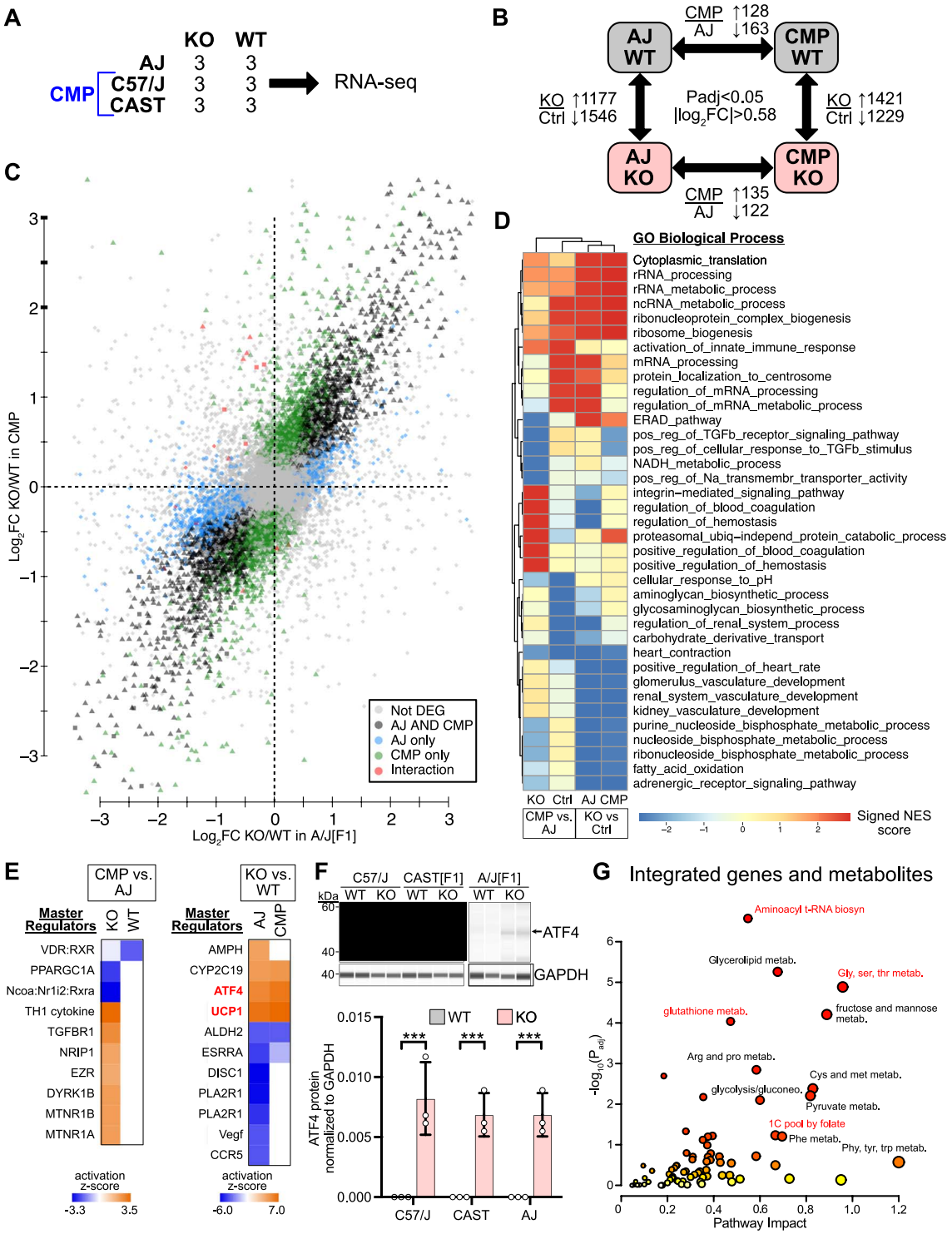


**Figure 5.** Transcriptomic and metabolomic characterization of *Taz* KO in permissive and non-permissive strain backgrounds. (**A**–**E**). Transcriptomic analysis of 2-month-old *Taz* KO and littermate control hearts in C57/J, CAST[F1] and A/J[F1] backgrounds. KO in C57/J represents $Taz^{flox/Y}$; Myh6Cre and in CAST[F1] and A/J[F1] represents $Taz^{KO/Y}$. KO in C57/J and CAST[F1] resulted in dilated CMP; these strains were pooled and labeled 'CMP'. (A) Experimental design of RNA-seq experiment, indicating number of biological replicates. (B) Analysis strategy. Four pairwise comparisons were performed. DEGs were defined as $P_{adj} < 0.05$ and $|\log_2 FC| > 0.58$. Number of up- and down-regulated genes is indicated for each comparison. (C) Comparison of gene expression change between KO and WT in CMP and A/J[F1] strains. Strain-dependent DEGs are colored green (DEG in CMP only) or blue (DEG in A/J[F1] only). Genes showing an interaction of strain and genotypes are colored red. (D) Top GO Biological Process terms enriched in each of the four comparisons. GO terms selected were the union of the top 10 terms from each comparison. KO versus WT enriched similar GO terms in A/J[F1] and CMP (right two columns). Strain-specific GO terms were distinct between KO and WT genotypes (left two columns). NES, normalized enrichment score. Positive and negative scores indicate enrichment in the numerator and denominator, respectively. (E) Master upstream regulator analysis by Ingenuity Pathway Analysis. Key pathways regulated by ATF4 and UCP1, highlighted in red, are activated in KO in both strains. Left plot, $P_{adj} < 10^{-3}$ and $|Z_{score}| > 2$. Right plot, $P_{adj} < 10^{-4}$ and $|Z_{score}| > 4$. (**F**) Confirmation of upregulation of ATF4 by capillary western. ATF4 levels were normalized to GAPDH. Two-way analysis of variance with Šidák's multiple comparison test. ***, $P < 0.001$. (**G**) Enriched pathways from Integration of targeted metabolomics with transcriptomics. Selected pathways are highlighted in red.

of datasets in the Ingenuity Knowledge Base, and ATF4 was in the top 5 percentile (Supplementary Material, Fig. S2C). UCP1 is expressed in brown adipose tissue, where it uncouples mitochondrial electron transport from ATP generation (26). Activation of similar downstream genes between UCP1 and *Taz* deficiency may reflect mitochondrial uncoupling. ATF4 is a central regulator of the integrated stress response, a conserved pathway that enables the cell to adapt to protein homeostasis defects, nutrient deprivation and oxidative stress (27). Upregulation of ATF4, a transcription factor, downregulates general mRNA translation and upregulations stress response genes to re-establish homeostasis. Among these upregulated pathways are genes involved in one-carbon metabolism and defense against oxidative stress (28). Capillary western blotting demonstrated markedly elevated levels of ATF4 in KO mice in C57/J, CAST[F1] and A/J[F1] strains (Fig. 5F). Upregulation of one-carbon metabolic pathway genes (Supplementary Material, Fig. S2B) further corroborated activation of ATF4 and the integrated stress response. Master upregulator analysis of genes differentially expressed between CMP and A/J[F1] identified reduced activity of PPARGC1A, a key regulator of metabolism and mitochondrial biogenesis, and increased activity of TGFBR1, a mediator of tissue inflammation and fibrosis, in CMP compared to A/J[F1] in KO hearts (Fig. 5E).

To further probe metabolic abnormalities caused by *Taz* deficiency, we performed targeted metabolomics analysis of 2- and 3.5-month-old C57/J $Taz^{KO/Y}$ and $Taz^{WT/Y}$ hearts. Biological triplicate samples clustered by group, and were separated by *Taz* genotype by principal component 1 (Supplementary Material, Fig. S3A). We pooled 2- and 3.5-month-old samples and focused on the effect of *Taz* genotype. From 172 metabolites quantified and analyzed, we identified 28 with significantly different levels between KO and WT (Supplementary Material, Fig. S3B, Table S2). Enriched pathways included 'Glycine and Serine Metabolism' and 'Mitochondrial beta oxidation of medium chain fatty acids', and 'Propanoate Metabolism' (Supplementary Material, Fig. S3C). Integrative analyses of genes and metabolites highlighted abnormalities in ATF4 signaling, aminoacyl-tRNA biosynthesis, glutathione metabolism, glycine and serine metabolism and 1C metabolism (Fig. 5G and Supplementary Material, Fig. S3D).

Together, the transcriptomic and metabolomic analysis identified genes and pathways affected by *Taz* KO. This analysis identified pathways perturbed by *Taz* KO in all strain tested backgrounds, such as those governed by ATF4 and UCP1. It also identified pathways uniquely perturbed in non-permissive compared to permissive strains, such as those governed by TGFBR1 and PPARGC1A.

### Strain-dependent effects of TAZ deficiency on mitochondrial morphology and dynamics

CL is critical for mitochondrial cristae structure, and abnormal mitochondrial morphology has been observed in both patient and murine samples (29,30). We used electron microscopy of 2-month-old ventricular myocardium to investigate the effect of *Taz* deficiency on mitochondrial morphology in different strain backgrounds. In both C57/J and CAST[F1] backgrounds, in which *Taz* deficiency causes CMP, mitochondria were small and had simplified cristae (Fig. 6A). In contrast, in the A/J[F1] background, where *Taz* deficiency does not cause CMP, we observed relatively well-preserved mitochondrial morphology. Quantitative analysis of electron microscopy (EM) images (Fig. 6B–E) confirmed reduced mitochondrial cross-sectional area of KO versus littermate control in C57/J and CAST[F1], but not in A/J[F1] (Fig. 6B). Cristae density was severely reduced in C57/J and CAST[F1]; in A/J[F1], it was also significantly reduced, although to a lesser degree. We also noticed that mitochondria were abnormally organized in KO in C57/J and CAST[F1] strains. In control mice, mitochondria are organized along myofibrils so that the large majority of mitochondria directly contact a sarcomere. In KO cardiomyocytes in C57/J and CAST[F1] strains, a significantly greater fraction of mitochondria form clusters in which many mitochondria fail to contact sarcomeres (Fig. 6A and D). In KO cardiomyocytes in A/J[F1], the fraction of mitochondria lacking sarcomere contact did not differ significantly from controls.

The presence of smaller mitochondria in C57/J and CAST[F1] KO hearts suggested impaired mitochondrial quality control through reduced mitochondrial fusion or increased fission, or impaired mitophagy. Using the RNA-seq data, we analyzed the expression of a panel of genes involved in mitochondrial fusion, fission or mitophagy (Fig. 6F). Many of these genes were dysregulated between KO versus control, especially in the CMP strains. We observed downregulation of *Opa1* and *Mfn2*, upregulation of *Mff* and downregulation of *Pink1*, *Atg2a* and *Atg9a*, which would be expected to reduce fusion, increase fission and reduce mitophagy, respectively.

To determine if strain background affected mitophagy in KO versus WT, we first quantified the overall level of autophagy by measurement of the autophagosomal marker LC3-II using capillary western. This showed an increase in bulk autophagy in KO in the A/J[F1] but not C57/J or CAST[F1] backgrounds (Supplementary Material, Fig. S4A and B). To directly measure mitophagy, we dissociated cardiomyocytes from 2-month-old CAST[F1] and A/J[F1] strains and treated them with a small molecule mitophagy dye, which localizes to mitochondria and increases red fluorescence when exposed to low pH within autophagosomes (31) (Fig. 6G). In the CAST[F1] genetic background, control cardiomyocytes had greater red fluorescence than KO (Fig. 6H). In contrast, red fluorescence increased in A/J[F1] KO compared to control cardiomyocytes. These data indicate that genetic background influences mitophagy in *Taz* KO, with mitophagy decreasing compared to littermate control in CAST[F1] and increasing in A/J[F1].

Together, these data suggest that genetic modifiers act downstream of CL to influence the effect of *Taz* deficiency on mitochondrial morphology and quality control. Specifically, the data associate development of CMP with fragmented mitochondrial morphology and reduced mitophagy.

## Discussion

We used mouse genetics to show that phenotypic manifestations of *Taz* deficiency and CL abnormalities are powerfully influenced by genetic modifiers. Within the same environment and with the same *Taz* mutation, different strain backgrounds altered phenotypic expression. Some strains appeared to be protective (A/J[F1]) or deleterious (C57/J) across multiple phenotypes, whereas the effects of other strains were phenotype specific. For example, CAST[F1] was the most deleterious for heart function, yet preserved normal treadmill endurance. These results suggest at least two classes of genetic modifiers—one class that operates across cell types to modulate the impact of *Taz* deficiency, and another class that operates in a cell type dependent manner. These classes suggest that different strains harbor distinct genetic modifiers.

Our results localize the level at which genetic modifiers in these strains act to modulate the impact of *Taz* deficiency. Prior results suggested that the effect of *Taz* ablation could be modulated by other genetic lesions in the CL biosynthetic or remodeling pathways. For example, KO or pharmacological inhibition of

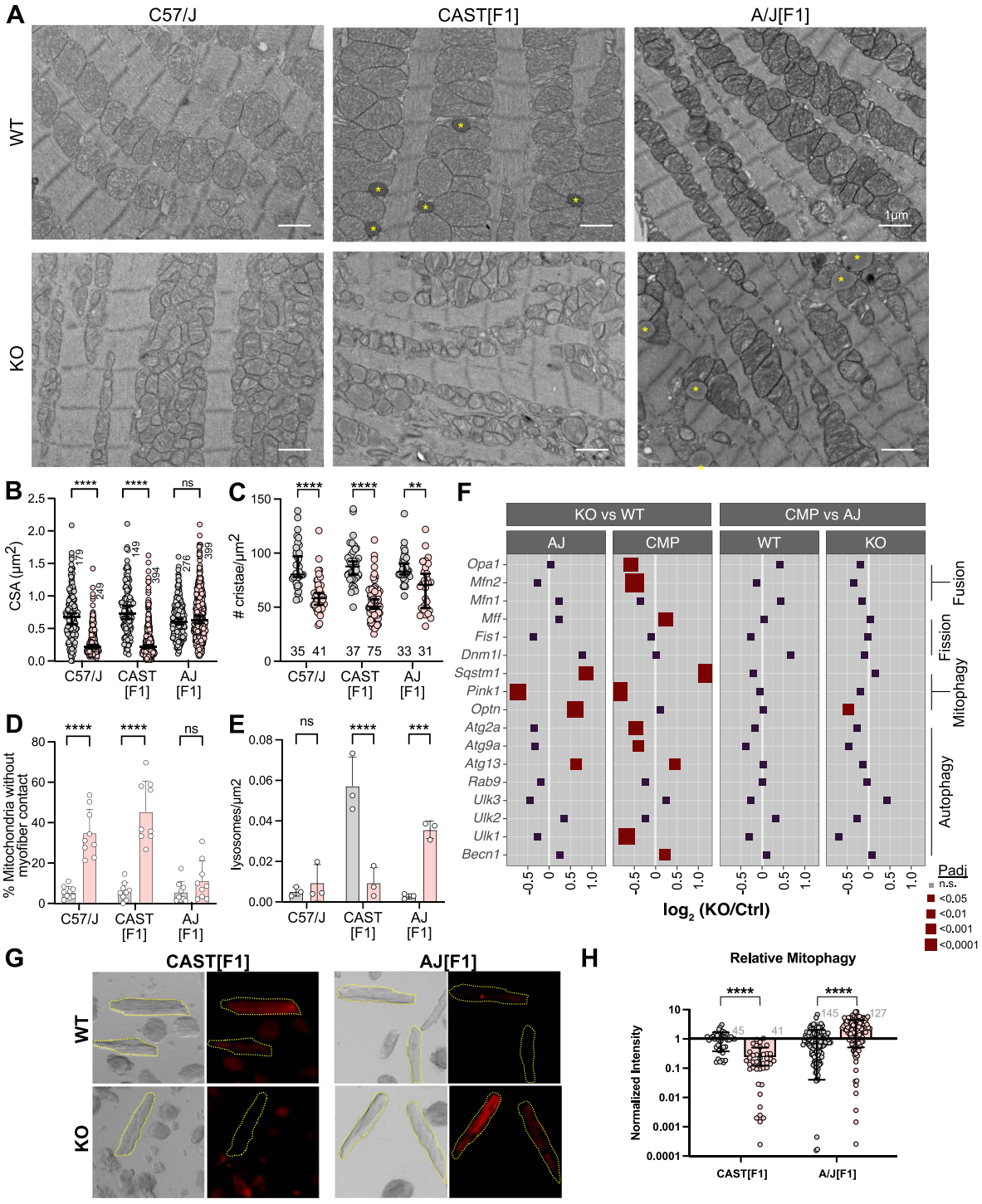


**Figure 6.** Impaired mitochondrial morphology and mitophagy in TAZ KO in non-permissive strain backgrounds. (**A**) Representative electron micrographs of 2-month-old TAZ KO and littermate control hearts in C57/J, CAST[F1] and A/J[F1] backgrounds. *, lysosomes. Bar, 1 $\mu$m. (**B**–**E**) Quantification of mitochondrial features from EM images. (B) Mitochondrial cross-sectional area (CSA). Lines indicate median ± 95% confidence interval (CI). Numbers indicate mitochondria quantified. Two-way analysis of variance (ANOVA) with Šidák's multiple comparison test. (C) Cristae density. Lines indicate median ± 95% CI. Each point is one mitochondrion. Five images from each of three animals per genotype were analyzed. Two-way ANOVA with Šidák's multiple comparison test. (D) Mitochondrial clustering. The fraction of mitochondria not in direct contact with a sarcomere on EM images was quantified. Each point represents one image. Two-way ANOVA with Šidák's multiple comparison test. (E) Lysosome density in cardiomyocytes. Lysosomes within cardiomyocytes were quantified from EM images. Each point represents one animal, with two to three images analyzed per animal. Two-way ANOVA with Šidák's multiple comparison test. (**F**) RNA expression of selected genes related to mitophagy. RNA-seq data are plotted, with size and color of each point indicating the genome-wide adjusted *P*-value. $P_{adj}$, adjusted *P*-value from DESeq2. (**G**) Mitophagy in dissociated cardiomyocytes. Dissociated adult cardiomyocytes from 2-month-old hearts were treated with Mitophagy Dye, a mitochondria-localized dye that increases red fluorescence within autophagosomes. Left, representative, corresponding bright field and fluorescent images. Right, quantification of mean fluorescence intensity of cardiomyocytes from CAST[F1] and A/J[F1] backgrounds. Fluorescence intensity was normalized to WT within each strain. Gray numbers indicate cardiomyocytes analyzed, from a minimum of three mice per group. Two-way ANOVA with Šidák's multiple comparison test. **, $P < 0.01$; ***, $P < 0.001$; ****, $P < 0.0001$. Ns, not significant.

phospholipase that converts CL to MLCL mitigated *Taz* deficiency in yeast or flies (32,33). However, our data show that *Taz* deficiency across the strains studied results in similar abnormalities of CL composition, indicating that these genetic modifiers act distally to influence the effect of altered CL composition on downstream processes. On the other hand, our data also suggest that the genetic modifiers act within mitochondria to modulate the effect of *Taz* deficiency on mitochondrial morphology and quality control. CL interacts with LC3 to mark mitochondria for mitophagy, and *Taz* depletion was previously shown to impair mitophagy (16,17). Despite *Taz* deficiency and abnormal CL composition, *Taz* KOs in the A/J[F1] background had greater autophagy and mitophagy than WT littermates and normal mitochondrial morphology. Elevated mitophagy in KO compared to control in A/J[F1] and the relatively preserved expression of mitophagy genes in this strain suggest that it is able to achieve robust mitochondrial quality control, which may contribute to protection from deleterious consequences of *Taz* ablation. In contrast, in the CMP CAST[F1] genetic background *Taz* KO resulted in reduced expression of mitophagy genes, lower mitophagy and small, fragmented mitochondria with simplified cristae, which together point to impaired mitochondrial quality control. Additional studies are required to test the hypothesis that genetic modifiers modulate cardiac phenotypes by altering mitochondrial quality control in the context of *Taz* KO and to determine mechanisms by which these genetic modifiers act. It will also be important to determine if similar findings for mitochondrial morphology and mitophagy extend to skeletal muscle and correlate with exercise capacity.

Our transcriptomic and metabolomic studies point to pathogenic effects of *Taz* mutation. The *Taz* KO gene expression signature shared features with activation of UCP1, a mitochondrial uncoupling protein. This finding is consistent with prior reports of reduced mitochondria membrane potential in *Taz* deficient cells (34,35), our observed downregulation of electron transport chain proteins in *Taz* KO cardiomyocytes and the known essential role of CL to stabilize respiratory chain supercomplexes (13,14). Furthermore, we observed strong activation of ATF4, a central effector of the integrated stress response. *Taz* mutation may activate this pathway through elevated reactive oxygen species (ROS) production or altered availability of key ribosomal machinery or aminoacyl-tRNAs. Based on its strong activation in both permissive and non-permissive strains, we anticipate that activation of ATF4 signaling is a compensatory mechanism. However, this will need to be clarified in future studies.

Our data provide clear evidence for strong genetic modifiers of *Taz* deficiency. The eight inbred strains used in this study are the founder lines for the Diversity Outbred strain (20). In ongoing studies, we are mapping the genetic modifiers by crossing $Taz^{KO/X}$ females to Diversity Outbred males and performing a genome wide association study on the F1 progeny to map the genetic modifiers. Identification of these modifiers and their mechanisms of action will illuminate the pathophysiology of Barth syndrome and identify novel therapies to mitigate the effects of *Taz* deficiency. Since these modifiers act to modulate the impact of aberrant CL composition, these modifiers and therapies will also be relevant to more common conditions associated with CL abnormalities, such as diabetes and heart failure (12).

# Materials and Methods

## Mice

Animal experiments were performed under protocols approved by the Boston Children's Hospital Institutional Animal Care and Use Committee. We studied male mice because Barth Syndrome (BTHS) is an X-linked disease that primarily affects males. Mice harboring the $Taz^{KO}$ and $Taz^{flox}$ alleles and polymerase chain reaction (PCR) genotyping protocols were described previously (19). These alleles have been backcrossed onto C57BL/6J for over seven generations. *Myh6Cre* was described previously (36) and obtained in the C57/J background (Jax #011038). WT mice in the eight inbred strains studied were purchased from Jackson Laboratories.

## Echocardiography

Echocardiography was performed monthly in unsedated mice using a Vevo 2100 (VisualSonics). After removal of chest hair, mice were held in a standard hand grip. M-mode short axis images were acquired for heart function measurements. Echocardiography was performed blinded to genotype and strain.

## Treadmill testing

We measured the exercise capacity of mice using a treadmill assay, as described previously (19,37). The treadmill is equipped with an electrified metal grid at the end of the moving belt to provide motivation for mice to run rather than rest on the grid. Animals were first trained to use treadmill and then run at 10 m/min for a total of 14 min. Mice were removed from the treadmill for exhaustion if they stayed on the shock grid for over 5 s or if they stayed on the shock grid for 2 s or more three times. The time mice spent on treadmill running was recorded. Data were analyzed using Cox-Mantel survival statistics.

## DEXA scanning

DEXA scanning (Piximus) was performed under isoflurane anesthesia.

## Histology

Cardiac or skeletal muscle samples were collected and fixed overnight in 4% paraformaldehyde solution at 4 ˚C. For histology analyses, samples were dehydrated through ethanol, embedded in paraffin and sectioned. WGA staining of dewaxed and rehydrated paraffin sections was performed using WGA conjugated to Alexa 555 (Life Technologies).

## Electron microscopy

Sample were fixed in EM fixative (2.5% Glutaraldehyde 2.5% Paraformaldehyde in 0.1 M sodium cacodylate buffer, pH 7.4) overnight at 4 ˚C. After fixation, tissue was washed in 0.1 M cacodylate buffer and postfixed with 1% Osmium tetroxide ($OsO_4$)/1.5% Potassium ferrocyanide ($KFeCN_6$) for 1 h. After washing in water three times, samples were incubated in 1% aqueous uranyl acetate for 1 h followed by two washes in water and subsequent dehydration in graded alcohol (10 min each; 50%, 70%, 90%, 2 × 10 min 100%). Subsequently, tissue samples were incubated in propylene oxide for 1 h and infiltrated ON in a 1:1 mixture of propylene oxide and TAAB Epon (Marivac Canada Inc. St. Laurent, Canada). On the next day, samples were embedded in TAAB Epon and polymerized at 60 ˚C for two additional days. Ultrathin sections (~60 nm) were cut on a Reichert Ultracut-S microtome, picked up on to copper grids stained with lead citrate and examined in a JEOL 1200EX Transmission electron microscope. Images were recorded with an AMT 2k CCD camera.

## CL analysis

Tissue was spiked with internal standard (Cardiolipin mix I, Avanti cat # LM6003) and lipids were extracted with chloroform/methanol. Extracted lipids were analyzed by Matrix Assisted

Laser Desorption/Ionization-Time of Flight Mass Spectrometry (38).

### Targeted metabolomics

A total of 258 metabolites were measured in mouse samples respectively using multiple reaction monitoring-based liquid chromatography-mass spectrometryPE (LC-MS) metabolite profiling techniques as previously described (39,40) (Supplementary Material, Table S2). Metabolomic data were annotated from compound names using MetaboAnalyst. Differential metabolite analysis, pathway enrichment and integration with DEGs were also performed using MetaboAnalyst or Ingenuity Pathway Analysis.

### Capillary westerns

Protein quantification was performed using a capillary electrophoresis device (WES, ProteinSimple). Primary antibodies used were: LC3/MAP1LC3A, Thermo Fisher Scientific, NB1002220SS; OXPHOS Rodent WB cocktail, Life Technologies, #458099; ATF4, Cell Signaling Technology, # 11815s and GAPDH, Life Technologies, #PA116777. Peak areas were quantified using Compass software (ProteinSimple).

### Mitophagy

Cardiomyocytes were dissociated by Langendorff perfusion with collagenase as described. Dissociated cardiomyocytes were treated with Mitophagy Dye (31) (Dojindo) and imaged using an epifluorescent/brightfield microscope (Keyence). Relative mitophagy was quantified by measuring the red fluorescent intensity.

### RNA-seq

Total RNA was extracted from snap-frozen tissue using Qiagen RNeasy RNA isolation kits. PolyA RNA purification, stranded RNA-seq library preparation and 150 nt paired end (PE) sequencing were performed by Beijing Genomics on the BGISEQ platform. Reads were aligned to GRCm38.p6 using HISAT (41). We obtained 16.5–45.2 M (mean 24.9 M) uniquely aligned read pairs per sample. Gene read counts were obtained using FeatureCounts (42). Differential expression analysis was performed using DESeq2 (43). Gene ontology analysis was performed using Gene Set Enrichment Analysis (24) or WebGestalt (44) (over-representation analysis). For Figure 5D, the union of the top 10 most significant GSEA GO Biological Process terms was selected to plot the heat map. The signed normalized enrichment score is the GSEA NES score multiplied by +1 for upregulated genes and −1 for downregulated genes. Causal network analysis was performed using Ingenuity Pathway Analysis (25).

### Statistics

Bar graphs indicate mean ± standard deviation (SD). Grouped point graphs show median and 95% confidence interval. Statistical analysis was performed in GraphPad Prism 9. Unless otherwise indicated, two-way analysis of variance was performed with Šidák's multiple comparison test to evaluate the effect of genotype within each strain. $P < 0.05$ was taken as statistically significant.

### Data sharing

RNA-seq data are available through GEO (GSE221675). Targeted metabolomics data are provided in Supplementary Material, Table S2.

## Supplementary Material

Supplementary Material is available at *HMG* online.

*Conflict of Interest statement*. The authors have no competing interests to declare.

## Funding

The U.S. Department of Defense (W81XWH2110445); National Institutes of Health (R01HL128694); the Barth Syndrome Foundation and charitable donations from Boston Children's Hospital Department of Cardiology.

## Authors' Contributions

S.W. and W.T.P. conceived of the project. S.W. planned the experiments, collected data and analyzed data. E.Y., E.K., N.M., A.H., Q.M. and H.W. collected and analyzed data. Y.X. and M.S. analyzed CL composition. X.S. and R.G. acquired metabolomics data. D.S. provided insightful discussions and key initial observations. W.T.P wrote the manuscript and S.W. and E.Y. edited it.

## References

1. Xu, Y., Malhotra, A., Ren, M. and Schlame, M. (2006) The enzymatic function of tafazzin. *J. Biol. Chem.*, **281**, 39217–39224.
2. Clarke, S.L.N., Bowron, A., Gonzalez, I.L., Groves, S.J., Newbury-Ecob, R., Clayton, N., Martin, R.P., Tsai-Goodman, B., Garratt, V., Ashworth, M. *et al.* (2013) Barth syndrome. *Orphanet J. Rare Dis.*, **8**, 23.
3. Roberts, A.E., Nixon, C., Steward, C.G., Gauvreau, K., Maisenbacher, M., Fletcher, M., Geva, J., Byrne, B.J. and Spencer, C.T. (2012) The Barth syndrome registry: distinguishing disease characteristics and growth data from a longitudinal study. *Am. J. Med. Genet. A*, **158A**, 2726–2732.
4. Taylor, C., Rao, E.S., Pierre, G., Chronopoulou, E., Hornby, B., Heyman, A. and Vernon, H.J. (2022) Clinical presentation and natural history of Barth syndrome: an overview. *J. Inherit. Metab. Dis.*, **45**, 7–16.
5. Chowdhury, S., Jackson, L., Byrne, B.J., Bryant, R.M., Cade, W.T., Churchill, T.L., Buchanan, J. and Taylor, C. (2022) Longitudinal observational study of cardiac outcome risk factor prediction in children, adolescents, and adults with Barth syndrome. *Pediatr. Cardiol.*, **43**, 1251–1263.
6. Ikon, N. and Ryan, R.O. (2017) Cardiolipin and mitochondrial cristae organization. *Biochim. Biophys. Acta Biomembr.*, **1859**, 1156–1163.
7. Xu, Y., Erdjument-Bromage, H., Phoon, C.K.L., Neubert, T.A., Ren, M. and Schlame, M. (2021) Cardiolipin remodeling enables protein crowding in the inner mitochondrial membrane. *EMBO J.*, **40**, e108428.
8. Wang, G., McCain, M.L., Yang, L., He, A., Pasqualini, F.S., Agarwal, A., Yuan, H., Jiang, D., Zhang, D., Zangi, L. *et al.* (2014) Modeling the mitochondrial cardiomyopathy of Barth syndrome with induced pluripotent stem cell and heart-on-chip technologies. *Nat. Med.*, **20**, 616–623.
9. Liu, X., Wang, S., Guo, X., Li, Y., Ogurlu, R., Lu, F., Prondzynski, M., de la Serna Buzon, S., Ma, Q., Zhang, D. *et al.* (2021) Increased reactive oxygen species-mediated $Ca^{2+}$/Calmodulin-dependent protein kinase II activation contributes to calcium handling abnormalities and impaired contraction in Barth syndrome. *Circulation*, **143**, 1894–1911.

10. Bertero, E., Nickel, A., Kohlhaas, M., Hohl, M., Sequeira, V., Brune, C., Schwemmlein, J., Abeßer, M., Schuh, K., Kutschka, I. *et al.* (2021) Loss of mitochondrial $Ca^{2+}$ uniporter limits inotropic reserve and provides trigger and substrate for arrhythmias in Barth syndrome cardiomyopathy. *Circulation*, **144**, 1694–1713.
11. Dudek, J., Cheng, I.-F., Balleininger, M., Vaz, F.M., Streckfuss-Bömeke, K., Hübscher, D., Vukotic, M., Wanders, R.J.A., Rehling, P. and Guan, K. (2013) Cardiolipin deficiency affects respiratory chain function and organization in an induced pluripotent stem cell model of Barth syndrome. *Stem Cell Res.*, **11**, 806–819.
12. Shi, Y. (2010) Emerging roles of cardiolipin remodeling in mitochondrial dysfunction associated with diabetes, obesity, and cardiovascular diseases. *J. Biomed. Res.*, **24**, 6–15.
13. Pfeiffer, K., Gohil, V., Stuart, R.A., Hunte, C., Brandt, U., Greenberg, M.L. and Schägger, H. (2003) Cardiolipin stabilizes respiratory chain supercomplexes. *J. Biol. Chem.*, **278**, 52873–52880.
14. Zhang, M., Mileykovskaya, E. and Dowhan, W. (2002) Gluing the respiratory chain together. Cardiolipin is required for supercomplex formation in the inner mitochondrial membrane. *J. Biol. Chem.*, **277**, 43553–43556.
15. Ban, T., Heymann, J.A.W., Song, Z., Hinshaw, J.E. and Chan, D.C. (2010) OPA1 disease alleles causing dominant optic atrophy have defects in cardiolipin-stimulated GTP hydrolysis and membrane tubulation. *Hum. Mol. Genet.*, **19**, 2113–2122.
16. Chu, C.T., Ji, J., Dagda, R.K., Jiang, J.F., Tyurina, Y.Y., Kapralov, A.A., Tyurin, V.A., Yanamala, N., Shrivastava, I.H., Mohammadyani, D. *et al.* (2013) Cardiolipin externalization to the outer mitochondrial membrane acts as an elimination signal for mitophagy in neuronal cells. *Nat. Cell Biol.*, **15**, 1197–1205.
17. Hsu, P., Liu, X., Zhang, J., Wang, H.-G., Ye, J.-M. and Shi, Y. (2015) Cardiolipin remodeling by TAZ/tafazzin is selectively required for the initiation of mitophagy. *Autophagy*, **11**, 643–652.
18. Kagan, V.E., Tyurin, V.A., Jiang, J., Tyurina, Y.Y., Ritov, V.B., Amoscato, A.A., Osipov, A.N., Belikova, N.A., Kapralov, A.A., Kini, V. *et al.* (2005) Cytochrome c acts as a cardiolipin oxygenase required for release of proapoptotic factors. *Nat. Chem. Biol.*, **1**, 223–232.
19. Wang, S., Li, Y., Xu, Y., Ma, Q., Lin, Z., Schlame, M., Bezzerides, V.J., Strathdee, D. and Pu, W.T. (2020) AAV gene therapy prevents and reverses heart failure in a murine knockout model of Barth syndrome. *Circ. Res.*, **126**, 1024–1039.
20. Churchill, G.A., Gatti, D.M., Munger, S.C. and Svenson, K.L. (2012) The diversity outbred mouse population. *Mamm. Genome*, **23**, 713–718.
21. Radavelli-Bagatini, S., Blair, A.R., Proietto, J., Spritzer, P.M. and Andrikopoulos, S. (2011) The New Zealand obese mouse model of obesity insulin resistance and poor breeding performance: evaluation of ovarian structure and function. *J. Endocrinol.*, **209**, 307–315.
22. Bashir, A., Bohnert, K.L., Reeds, D.N., Peterson, L.R., Bittel, A.J., de Las Fuentes, L., Pacak, C.A., Byrne, B.J. and Cade, W.T. (2017) Impaired cardiac and skeletal muscle bioenergetics in children, adolescents, and young adults with Barth syndrome. *Physiol Rep*, **5**, e13130.
23. Frazer, K.A., Eskin, E., Kang, H.M., Bogue, M.A., Hinds, D.A., Beilharz, E.J., Gupta, R.V., Montgomery, J., Morenzoni, M.M., Nilsen, G.B. *et al.* (2007) A sequence-based variation map of 8.27 million SNPs in inbred mouse strains. *Nature*, **448**, 1050–1053.
24. Subramanian, A., Tamayo, P., Mootha, V.K., Mukherjee, S., Ebert, B.L., Gillette, M.A., Paulovich, A., Pomeroy, S.L., Golub, T.R., Lander, E.S. *et al.* (2005) Gene set enrichment analysis: a knowledge-based approach for interpreting genome-wide expression profiles. *Proc. Natl. Acad. Sci. U. S. A.*, **102**, 15545–15550.
25. Krämer, A., Green, J., Pollard, J., Jr. and Tugendreich, S. (2014) Causal analysis approaches in ingenuity pathway analysis. *Bioinformatics*, **30**, 523–530.
26. Nicholls, D.G. (2021) Mitochondrial proton leaks and uncoupling proteins. *Biochim. Biophys. Acta Bioenerg.*, **1862**, 148428.
27. Costa-Mattioli, M. and Walter, P. (2020) The integrated stress response: from mechanism to disease. *Science*, **368**, eaat5314.
28. Celardo, I., Lehmann, S., Costa, A.C., Loh, S.H. and Miguel Martins, L. (2017) dATF4 regulation of mitochondrial folate-mediated one-carbon metabolism is neuroprotective. *Cell Death Differ.*, **24**, 638–648.
29. Acehan, D., Xu, Y., Stokes, D.L. and Schlame, M. (2007) Comparison of lymphoblast mitochondria from normal subjects and patients with Barth syndrome using electron microscopic tomography. *Lab. Investig.*, **87**, 40–48.
30. Soustek, M.S., Falk, D.J., Mah, C.S., Toth, M.J., Schlame, M., Lewin, A.S. and Byrne, B.J. (2011) Characterization of a transgenic short hairpin RNA-induced murine model of Tafazzin deficiency. *Hum. Gene Ther.*, **22**, 865–871.
31. Iwashita, H., Torii, S., Nagahora, N., Ishiyama, M., Shioji, K., Sasamoto, K., Shimizu, S. and Okuma, K. (2017) Live cell imaging of mitochondrial autophagy with a novel fluorescent small molecule. *ACS Chem. Biol.*, **12**, 2546–2551.
32. Ye, C., Lou, W., Li, Y., Chatzispyrou, I.A., Hüttemann, M., Lee, I., Houtkooper, R.H., Vaz, F.M., Chen, S. and Greenberg, M.L. (2014) Deletion of the cardiolipin-specific phospholipase Cld1 rescues growth and life span defects in the tafazzin mutant: implications for Barth syndrome. *J. Biol. Chem.*, **289**, 3114–3125.
33. Malhotra, A., Edelman-Novemsky, I., Xu, Y., Plesken, H., Ma, J., Schlame, M. and Ren, M. (2009) Role of calcium-independent phospholipase A2 in the pathogenesis of Barth syndrome. *Proc. Natl. Acad. Sci. U. S. A.*, **106**, 2337–2341.
34. Jiang, F., Ryan, M.T., Schlame, M., Zhao, M., Gu, Z., Klingenberg, M., Pfanner, N. and Greenberg, M.L. (2000) Absence of cardiolipin in the crd1 null mutant results in decreased mitochondrial membrane potential and reduced mitochondrial function. *J. Biol. Chem.*, **275**, 22387–22394.
35. Xu, Y., Sutachan, J.J., Plesken, H., Kelley, R.I. and Schlame, M. (2005) Characterization of lymphoblast mitochondria from patients with Barth syndrome. *Lab. Investig.*, **85**, 823–830.
36. Agah, R., Frenkel, P.A., French, B.A., Michael, L.H., Overbeek, P.A. and Schneider, M.D. (1997) Gene recombination in postmitotic cells. Targeted expression of Cre recombinase provokes cardiac-restricted, site-specific rearrangement in adult ventricular muscle in vivo. *J. Clin. Invest.*, **100**, 169–179.
37. Castro, B. and Kuang, S. (2017) Evaluation of muscle performance in mice by treadmill exhaustion test and whole-limb grip strength assay. *Bio-protocol*, **7**, e2237.
38. Xu, Y., Phoon, C.K.L., Berno, B., D'Souza, K., Hoedt, E., Zhang, G., Neubert, T.A., Epand, R.M., Ren, M. and Schlame, M. (2016) Loss of protein association causes cardiolipin degradation in Barth syndrome. *Nat. Chem. Biol.*, **12**, 641–647.
39. Kimberly, W.T., O'Sullivan, J.F., Nath, A.K., Keyes, M., Shi, X., Larson, M.G., Yang, Q., Long, M.T., Vasan, R., Peterson, R.T. *et al.* (2017) Metabolite profiling identifies anandamide as a biomarker of nonalcoholic steatohepatitis. *JCI Insight*, **2**. https://doi.org/10.1172/jci.insight.92989.
40. Wang, T.J., Larson, M.G., Vasan, R.S., Cheng, S., Rhee, E.P., McCabe, E., Lewis, G.D., Fox, C.S., Jacques, P.F., Fernandez, C. *et al.* (2011) Metabolite profiles and the risk of developing diabetes. *Nat. Med.*, **17**, 448–453.

41. Kim, D., Langmead, B. and Salzberg, S.L. (2015) HISAT: a fast spliced aligner with low memory requirements. *Nat. Methods*, **12**, 357–360.
42. Liao, Y., Smyth, G.K. and Shi, W. (2014) featureCounts: an efficient general purpose program for assigning sequence reads to genomic features. *Bioinformatics*, **30**, 923–930.
43. Love, M.I., Huber, W. and Anders, S. (2014) Moderated estimation of fold change and dispersion for RNA-seq data with DESeq2. *Genome Biol.*, **15**, 550.
44. Liao, Y., Wang, J., Jaehnig, E.J., Shi, Z. and Zhang, B. (2019) WebGestalt 2019: gene set analysis toolkit with revamped UIs and APIs. *Nucleic Acids Res.*, **47**, W199–W205.